Evolution of magnetic phases in single crystals of $SrFe_{1-x}Co_xO_3$ solid solution

Y. W. Long,[1,2,*] Y. Kaneko,[1,3] S. Ishiwata,[4] Y. Tokunaga,[3] T. Matsuda,[4] H. Wadati,[4] Y. Tanaka,[5] S. Shin,[5,6] Y. Tokura,[1,3,4] and Y. Taguchi[3]

[1]*Multiferroics Project, Exploratory Research for Advanced Technology, Japan Science and Technology Agency, c/o RIKEN Advanced Science Institute, Wako 351-0198, Japan*

[2]*Beijing National Laboratory for Condensed Matter Physics, Institute of Physics, Chinese Academy of Sciences, Beijing 100190, China*

[3]*Cross-Correlated Materials Research Group (CMRG) and Correlated Electron Research Group (CERG), RIKEN Advanced Science Institute, Wako 351-0198, Japan*

[4]*Department of Applied Physics and Quantum-Phase Electronics Center (QPEC), University of Tokyo, Hongo, Tokyo 113-8656, Japan*

[5]*RIKEN SPring-8 Center, Sayo, Hyogo 679-5148, Japan*

[6]*The Institute for Solid State Physics, University of Tokyo, Kashiwa, Chiba 277-8581, Japan*

(Received 9 April 2012; revised manuscript received 12 July 2012; published 27 August 2012)

Single crystals of $SrFe_{1-x}Co_xO_3$ solid solution with high valence ions (Fe^{4+}/Co^{4+}) were synthesized by combining floating-zone and high-pressure oxygen-annealing techniques. As the Co content (x) is increased, the ground state changes from the helimagnetic state ($x \leqslant 0.05$) through cluster glass to the ferromagnetic state ($x \geqslant 0.2$), with a high Curie temperature ranging between 245 and 337 K. We found that, within the helimagnetic state ($x \leqslant 0.05$), several different magnetic phases, which possibly reflect versatile three-dimensional helical orders with multiple wave vectors, emerge depending on temperature and magnetic field strength. In addition, we observed Co-concentration–dependent systematic evolution of the complex magnetic phase diagram. Resonant soft x-ray diffraction measurements revealed a gradual decrease in the wave vector of the helix toward the ferromagnetic phase.

DOI: 10.1103/PhysRevB.86.064436 PACS number(s): 75.30.−m, 75.47.−m, 72.80.Ga

I. INTRODUCTION

Compounds with helimagnetic (HM) structure exhibit interesting physical properties.[1–6] For the emergence of HM structure, there are several mechanisms. The first one is based on the Dzyaloshinskii-Moriya (DM) interaction as realized in compounds with non-centrosymmetric crystal structure.[1,2] The second one is the frustration among several competing exchange interactions.[3,4] The third one is mediated by conduction electrons, as proposed for rare earth metals or the double exchange system with negative charge transfer energy.[6] $SrFeO_3$, with a simple cubic Pm-$3m$ lattice symmetry, is a well-known example showing a HM structure, and it provides a good arena to study the complex helimagnetism.[7,8] Neutron diffraction has revealed that a HM structure is established at $T_N = 134$ K, and the wave vector is parallel to the $\langle 111 \rangle$ direction.[9,10] The origin of this HM structure is attributed to the competing nearest-neighbor (NN) ferromagnetic (FM) and next-NN antiferromagnetic interactions,[10] or to the double exchange interaction with the negative charge transfer energy or oxygen p-hole character.[6] It is known that the HM structure of $SrFeO_3$ is easily turned into the FM state by the partial substitution of Fe with Co.[8,11] Figure 1 shows a magnetic phase diagram of the $SrFe_{1-x}Co_xO_3$ solid solution obtained from our single-crystal samples in this study. When the Co content x is increased to 0.05, the T_N is quickly suppressed to 105 K, and then FM cluster glass (CG) behavior appears for a Co content range around $x = 0.1$. In the region with $x \geqslant 0.2$, a long-range FM state emerges, and the highest FM Curie temperature (T_C) is around 337 K for $SrFe_{0.4}Co_{0.6}O_3$. The end compound $SrCoO_3$ is also a FM metal at room temperature.[12]

In the case of undoped $SrFeO_3$, the system undergoes multiple magnetic transitions at different temperatures and fields.[13–16] As shown in Fig. 2(a), five HM phases (phase I–V) have been observed in a previous study for the fully oxidized single crystalline sample in high magnetic fields;[16] three magnetic transitions are observed at low fields around $T_{N1} \approx 56$ K, $T_{N2} \approx 110$ K, and $T_{N3} = T_N \approx 134$ K. Furthermore, at higher fields, two field-induced magnetic phases are found. In phases I and II, but not in phase III, an unconventionally enhanced anomalous Hall effect is observed, implying the presence of nontrivial spin textures.[16] These magnetic transitions can be unambiguously identified by magnetization and transport measurements, but the detailed magnetic structures in these phases are still unclear at present, although they certainly possess the helix-related orders with very similar modulation vectors (q-vectors), as found in neutron diffraction experiment for $SrFeO_3$ without a magnetic field.[16,17] In order to understand the properties of the complex magnetic phases, it will be useful to finely control the Co concentration and study the evolution of these magnetic phases in temperature-field planes.

Although polycrystalline samples of $SrFe_{1-x}Co_xO_3$ solid solution have been investigated in previous studies,[8,18–21] there is no report on the detailed evolution of magnetic phases with light Co concentration. In addition, single crystalline samples are indispensable to observe the intrinsic properties that might be easily hidden by the effect of grain boundaries. However, single-crystal samples of $SrFe_{1-x}Co_xO_3$ solid solution have not been available thus far. Due to the high valence state of Fe^{4+}/Co^{4+} ions in this system, high oxygen pressure is needed to synthesize the compounds without oxygen vacancies. Recently, a two-step method for synthesizing fully oxidized large-size single crystals of high-metal-valence perovskites has been developed.[12,16,22] By means of this technique, high-quality $SrFeO_3$ and $SrCoO_3$ crystals with stoichiometric oxygen content were obtained.[12,16] In this work, we synthesized $SrFe_{1-x}Co_xO_3$ single crystals with finely controlled Co concentration using a similar method,

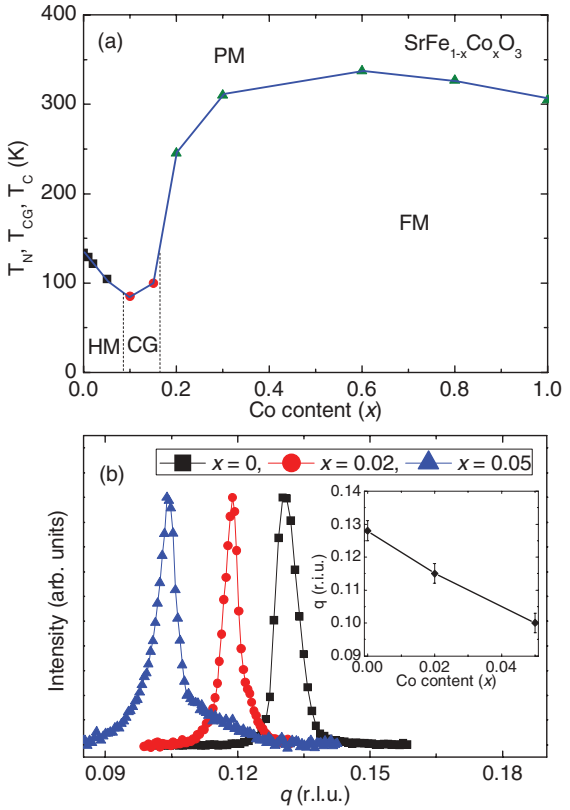

FIG. 1. (Color online) (a) Magnetic phase diagram of single crystalline $SrFe_{1-x}Co_xO_3$ solid solution obtained in this study. PM, HM, CG, and FM denote paramagnetic, helimagnetic, cluster glass, and ferromagnetic phase, respectively. T_N, T_{CG}, and T_C denote the HM, CG, and FM transition temperature and are plotted with black square, red circle, and blue triangle, respectively. The vertical dotted lines represent approximate positions of phase boundaries. (b) Magnetic diffraction peaks of $SrFe_{1-x}Co_xO_3$ ($x = 0$, 0.02, 0.05) at 40 K obtained by resonant soft x-ray diffraction (RSXD) measurements. The inset to (b) shows the x dependence of q, with $\boldsymbol{q} = (q\,q\,q)$ being the scattering vector. The vertical bars indicate the variation of the q value within measured temperature range (40–150 K).

and investigated systematic changes of the multiple magnetic phases with increasing Co content. Thus, composition (x)–dependent magnetic phase diagrams were obtained in the temperature vs magnetic-field planes for $SrFe_{1-x}Co_xO_3$. In addition, we clarified the change in q-vector of the helix by using resonant soft x-ray diffraction (RSXD), which has proven to be a powerful tool to investigate magnetic structures, as recently used to study the magnetically ordered states in 3d transition metal oxides.[23–27]

II. EXPERIMENTAL METHODS

High-purity $SrCO_3$, Fe_2O_3, and Co_3O_4 were used as starting materials for sample synthesis. First, oxygen-deficient $SrFe_{1-x}Co_xO_{2.5}$ polycrystalline samples with brownmillerite-type structure were prepared through a standard solid-state reaction method,[28–30] and then single crystals were grown from the polycrystalline rods by using a floating-zone method in flowing Ar gas, as described elsewhere.[12] These oxygen-deficient crystals were treated in an oxidizing atmosphere at

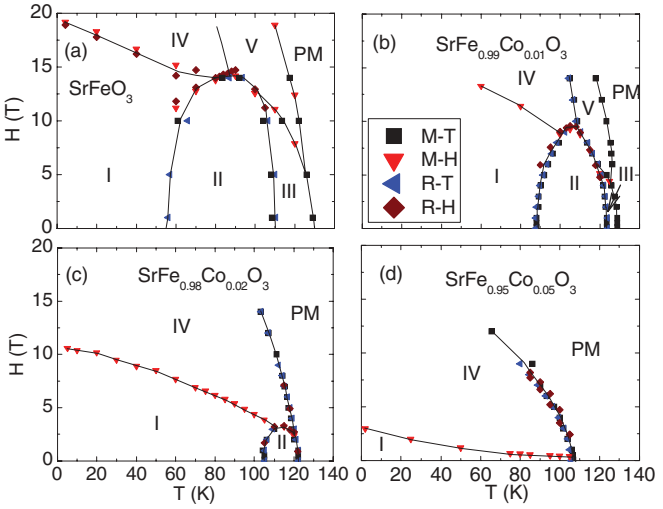

FIG. 2. (Color online) Magnetic phase diagrams for (a) $SrFeO_3$, (b) $SrFe_{0.99}Co_{0.01}O_3$, (c) $SrFe_{0.98}Co_{0.02}O_3$, and (d) $SrFe_{0.95}Co_{0.05}O_3$ in the plane of temperature vs magnetic field. Phase boundaries are determined from the temperature variation of magnetization (M-T) and resistivity (R-T) collected in heating runs, and also from the field variation of magnetization (M-H) and resistivity (R-H) obtained in field-increasing runs. The phase diagram for $SrFeO_3$ is reproduced from Ref. 16.

6.5 GPa and 973–1073 K for 1 h by using a cubic-anvil–type high-pressure apparatus. For the high-pressure annealing process, excess $KClO_4$ was used as oxygen source. The crystal quality was checked by a back-reflection Laue method, and the phase purity and lattice parameters were examined by using an x-ray diffractometer with Cu-K_α radiation (40 kV, 300 mA).

Temperature dependence of magnetization was measured with a superconducting quantum interference device (SQUID) magnetometer (Quantum Design Magnetic Property Measurement System [MPMS]) in zero-field-cooling (ZFC) and/or field-cooling (FC) modes at different fields. The ZFC process was used to measure the field dependence of magnetization at different temperatures. Temperature and field dependence of resistivity was measured by using a Quantum Design Physical Property Measurement System PPMS at constant fields and temperatures, respectively. The values of the magnetoresistance (MR) ratio were calculated using the following equation: MR ratio $= [\rho(\mathrm{H}) - \rho(0)]/\rho(0)$, where $\rho(\mathrm{H})$ and $\rho(0)$ denote resistivity values at a magnetic field H and zero field, respectively. The alternating current (ac) magnetic susceptibility was also measured using a PPMS.

The magnetic q-vectors of $SrFe_{1-x}Co_xO_3$ ($x = 0$, 0.02, 0.05) were investigated by using resonant soft x-ray diffraction. Measurements of RSXD were carried out using an ultrahigh-vacuum diffractometer equipped at the beamline 17SU, SPring-8, Japan.[31] The incident photon energy was tuned to the Fe L_3 edge (=708 eV). The polarization of the incident x ray was circular, and we obtained the same results from right- and left-handed circular polarization.

III. RESULTS AND DISCUSSION

The samples after high-oxygen-pressure treatment proved to be of high-quality $SrFe_{1-x}Co_xO_3$ single crystals. Figure 3(a)

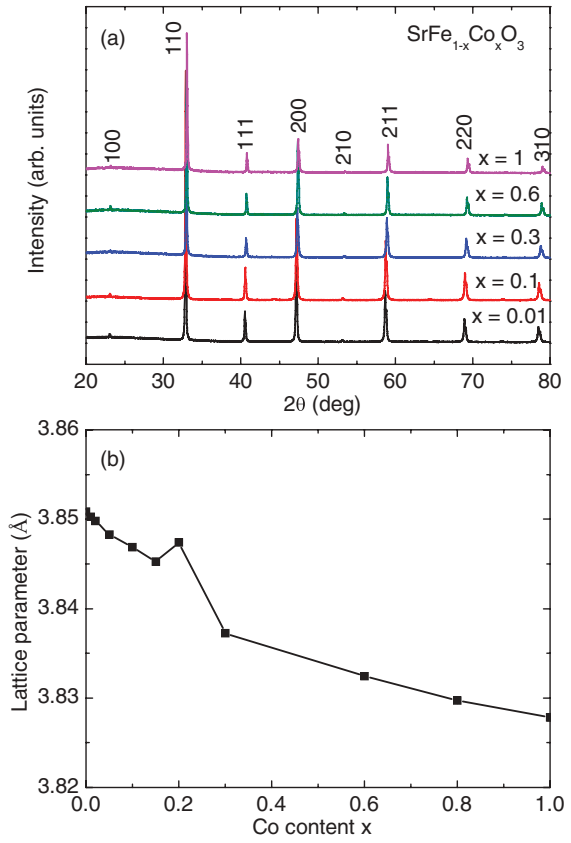

FIG. 3. (Color online) Room-temperature (a) powder x-ray diffraction patterns, and (b) lattice parameter as a function of Co content x for $SrFe_{1-x}Co_xO_3$ solid solution. The error bars in (b) are within the symbol size.

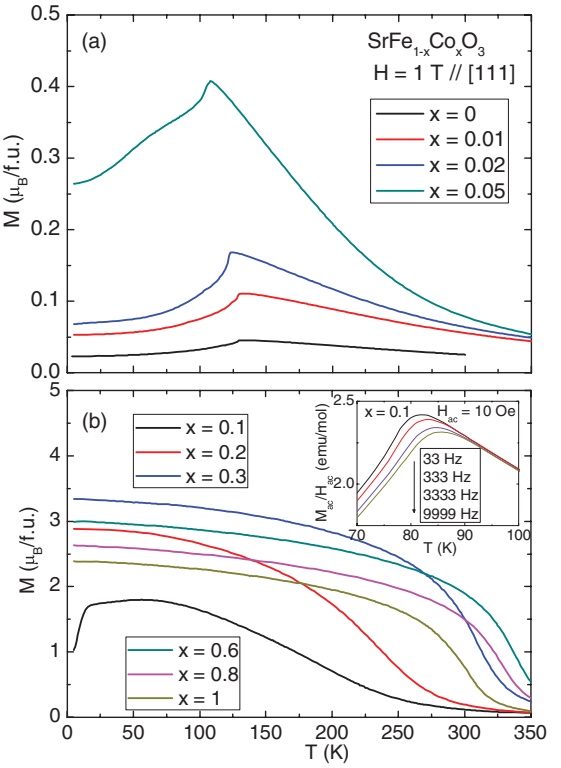

FIG. 4. (Color online) Temperature dependence of magnetization for (a) helimagnetic and (b) cluster glass and ferromagnetic crystals of $SrFe_{1-x}Co_xO_3$. The data were taken at H = 1 T applied along [111] direction. The inset to (b) shows the ac magnetic susceptibility of $SrFe_{0.9}Co_{0.1}O_3$ measured at several different frequencies with ac field amplitude of 10 Oe.

shows powder x-ray diffraction patterns measured at room temperature (RT) for several representative compounds. All the diffraction peaks can be well indexed in terms of a simple cubic Pm-$3m$ space group. The calculated lattice constant is plotted against x in Fig. 3(b). Due to the smaller ionic radius of Co^{4+} as compared to Fe^{4+},[32] the lattice parameter monotonically decreases with increasing Co content, except for a compound with $x = 0.2$, where the magnetism changes from cluster glass behavior to long-range FM ordering (Figs. 1 and 4). Since the lattice parameters are obtained at RT, where the $x = 0.2$ crystal is paramagnetic while the $x \geqslant 0.3$ crystals are ferromagnetic, the lattice anomaly observed at $x = 0.2$ is indicative of a strong magneto-volume effect as discussed in Ref. 8.

Figure 1(b) shows the magnetic peaks of $SrFeO_3$, $SrFe_{0.98}Co_{0.02}O_3$, and $SrFe_{0.95}Co_{0.05}O_3$ obtained by RSXD in the HM phase at 40 K. The scattered intensity is plotted as a function of q; here, scattering vector is denoted as (q, q, q). Co-content (x) dependence of the peak position is shown in the inset of Fig. 1(b). The q value decreases with increasing x, which means the periodicity of the spin spiral increases as x is increased. This result indicates that the increase in Co concentration enhances the FM correlations.

Figure 4 shows the temperature dependence of magnetization measured at 1 T in a zero-field-cooled warming run. A cusp is clearly observed in each sample with $x \leqslant 0.05$, and this temperature, assigned to T_N (the onset of HM ordering), is plotted in Fig. 1. Obviously, with increasing Co concentration, the HM-ordering temperature is reduced, and the magnitude of magnetization gradually increases. This means that the introduction of Co ions reinforces the FM correlation in these HM compounds, in accord with the results of RSXD. As the Co content x is increased to 0.1, the helical spin state is suppressed, and instead the compound displays a cluster glass behavior, as characterized by a gradual increase in the direct current (dc) magnetization around 250 K as well as by the frequency-dependent behavior of ac susceptibility (see Fig. 4 and the inset). As the Co concentration is further increased to $x \geqslant 0.2$, a long-range ordered FM state with high Curie temperature (>245 K) emerges, as shown in Fig. 4(b). In the present system with high valence ions (Fe^{4+}/Co^{4+}), theoretical as well as experimental studies have revealed the presence of large negative charge transfer energy and the holes on oxygen p-bands.[33–35] In $SrCoO_3$, the FM ordering was suggested to originate from the double-exchange–like interaction between Co spins and oxygen holes.[34] Also in the case of solid solution $SrFe_{1-x}Co_xO_3$, the double-exchange interaction is expected to play a key role for the emergence of the FM state.

Corresponding to the HM ordering in the compounds with $x \leqslant 0.05$, the magnetization is found to be H-linear for $|H| \leqslant 7$ T, as shown in Fig. 5(a). The slight hysteresis observed in the $x = 0.05$ crystal may signal the presence of a short-range FM

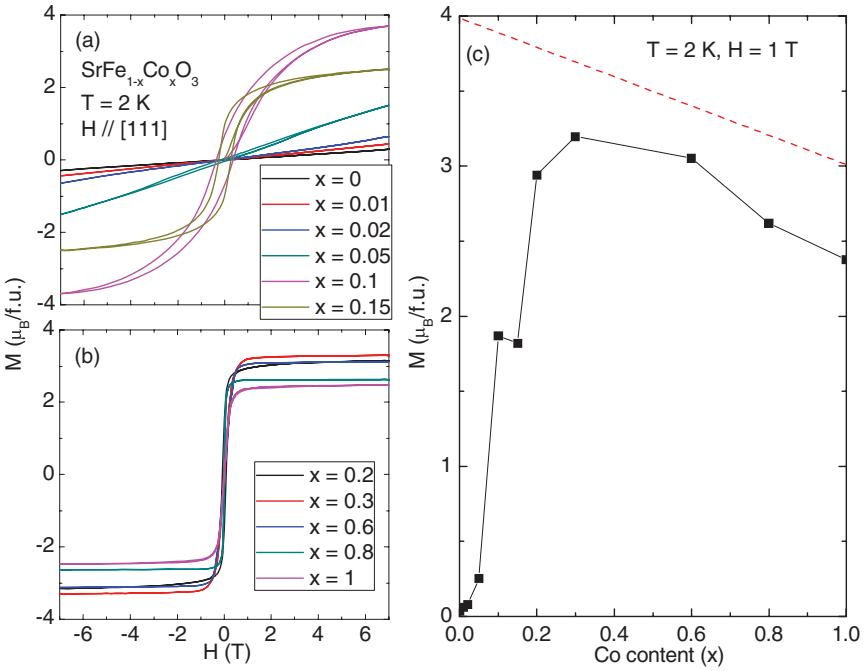

FIG. 5. (Color online) Field dependence of magnetization for (a) helimagnetic ($x \leqslant 0.05$) and cluster glass ($x = 0.1$ and 0.15), and (b) ferromagnetic crystals of $SrFe_{1-x}Co_xO_3$ measured at 2 K with field along [111] direction. (c) Co concentration (x) dependence of magnetization at 2 K and 1 T collected in a field-decreasing process. Dashed line represents the magnetization value at B-site expected for the average of high-spin Fe^{4+} ($t_{2g}{}^3e_g{}^1$; $S = 2$) and intermediate-spin Co^{4+} ($t_{2g}{}^4e_g{}^1$; $S = 3/2$).

correlation between Co and Fe ions. In accordance with the picture of cluster glass, *S*-shaped magnetization accompanied by a considerable hysteresis is found in the crystals with $x = 0.1$ and 0.15. Moreover, the magnetization does not saturate, even at 7 T. On the other hand, in the FM compounds with $x \geqslant 0.2$, the magnetization rapidly increases with increasing field and becomes saturated at about 1 T (Fig. 5(b)). In contrast to the CG samples, the magnetic hysteresis in these FM compounds is very small. For instance, the coercive field observed in $SrCoO_3$ is as small as 0.03 T.[12]

Figure 5(c) shows the Co concentration (x) dependence of the magnetization value obtained at 1 T (above the coercive field values of FM compounds) and 2 K. In the HM region ($x \leqslant 0.05$), the magnetization is slightly enhanced by increasing Co concentration, in accord with the result of temperature dependence (Fig. 4(a)). Upon the magnetic transition from AFM to CG ($x = 0.1$–0.15), the moment shows a sharp increase. The magnetization values for $x = 0.10$ and 0.15 compounds (collected in a field-decreasing process) almost coincide with each other, although the shape of the M-H curves, shown in Fig. 5(c), is slightly different, reflecting the transitional composition region between HM and FM states. In the FM phase ($x \geqslant 0.2$), the magnetization reaches a maximum at $x = 0.3$, and then gradually decreases as x is further increased. As recently revealed for a $SrCoO_3$ single crystal, the spin state of Co^{4+} is close to an intermediate spin ($t_{2g}{}^4e_g{}^1$, $S = 3/2$),[12] in agreement with theoretical prediction.[34] On the other hand, the Fe^{4+} ion possesses a high spin state ($t_{2g}{}^3e_g{}^1$, $S = 2$) with a larger spin moment compared to the intermediate-spin Co^{4+} state.[16] This simple picture basically explains the gradual decrease in magnetization with increasing Co concentration in the FM region, as represented in Fig. 5(c).

In the present $SrFe_{1-x}Co_xO_3$ system, all the compounds exhibit metallic behavior while the magnetism changes from HM through CG to FM. Figure 6 shows the electrical resistivity as a function of temperature in zero magnetic field for several compositions. For the CG crystal with $x = 0.1$, there is no clear anomaly in the temperature dependence of resistivity. On the other hand, for the HM and FM crystals, clear anomalies are observed at the magnetic transition temperatures as shown by the arrows, suggesting considerable coupling between magnetism and charge transport. In particular, in the $x = 0.02$ crystal, there exist two anomalies, which correspond to complex and successive transitions in the HM compounds, as observed in $SrFeO_3$.[16] We therefore focused on the magnetic and transport properties for the HM compounds in detail at various temperatures and magnetic fields. The slightly doped $SrFe_{0.99}Co_{0.01}O_3$ can be used as an example to show these interesting properties of the helimagnet.

Figure 7(a) shows the temperature dependence of magnetic susceptibility and its temperature derivative for $SrFe_{0.99}Co_{0.01}O_3$ measured at a low field of 0.1 T. Obviously, three magnetic transitions are observed at T_{N1} (88 K), T_{N2} (123 K), and T_{N3} (129 K), respectively. This behavior is similar

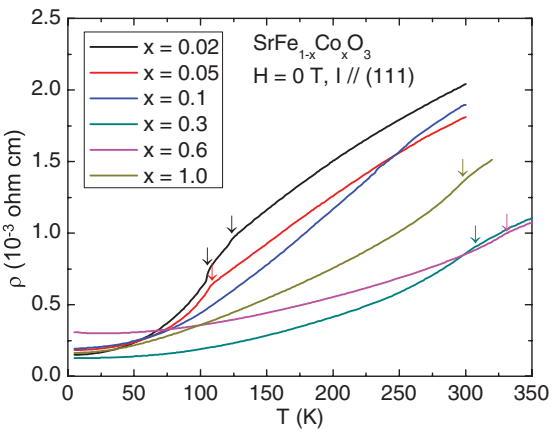

FIG. 6. (Color online) Temperature dependence of resistivity for several representative compounds of $SrFe_{1-x}Co_xO_3$. The data were collected at zero field with current parallel to (111) plane. Arrows indicate magnetic anomalies.

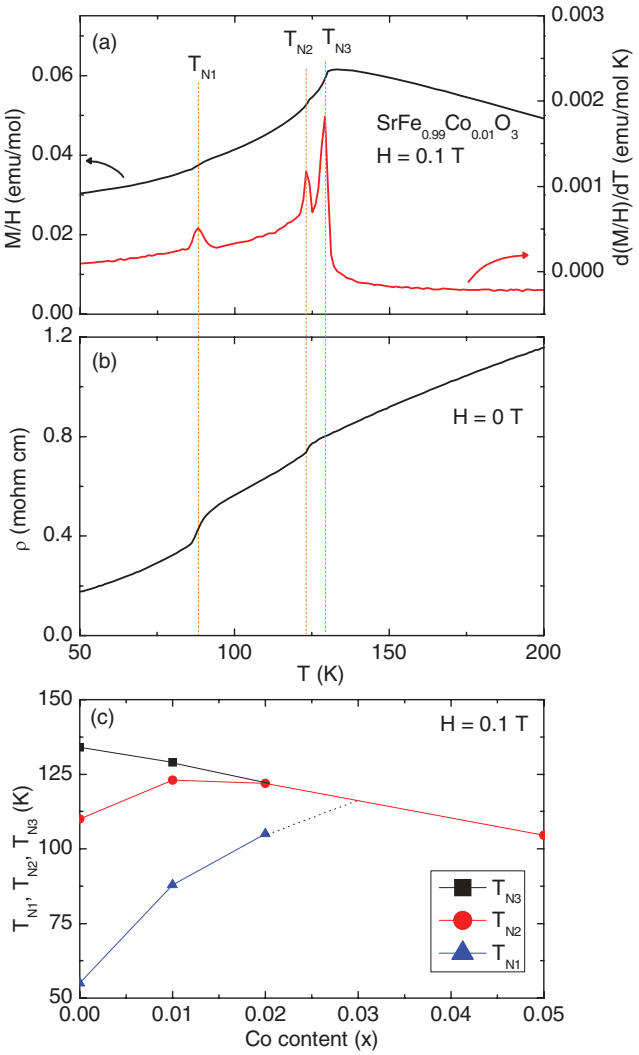

FIG. 7. (Color online) Temperature dependence of (a) susceptibility and its temperature derivative at 0.1 T, and (b) resistivity at zero field for $SrFe_{0.99}Co_{0.01}O_3$. (c) Successive magnetic-transition temperatures as a function of Co content at a low field (H = 0.1 T).

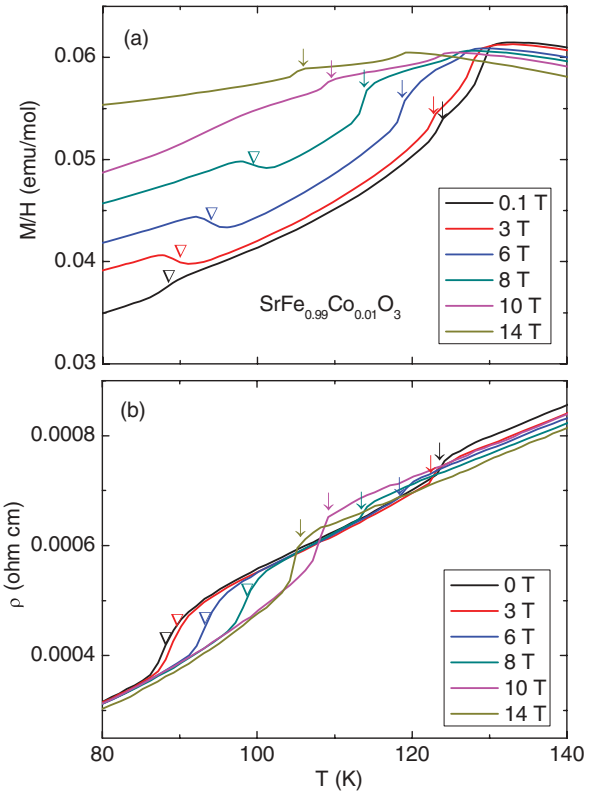

FIG. 8. (Color online) Temperature dependence of (a) susceptibility and (b) resistivity of $SrFe_{0.99}Co_{0.01}O_3$ at different fields up to 14 T. The arrows and triangles represent the phase-transition temperatures T_{N2} and T_{N1}, respectively.

to the evolution of the magnetic phases in $SrFeO_3$,[14–16] for which neutron diffraction has been performed.[9,16,17] Nevertheless, the changes in spin structure at the phase-transition temperatures T_{N1} and T_{N2} remain elusive; the magnetic wave vector value itself changes little upon these transitions, in spite of rather sharp changes in magnetization and charge transport as shown in the following. Although the long-range HM ordering is established at T_{N3}, no clear resistivity anomaly takes place at this critical temperature. The reason for this is not clear at present, but one possible origin is the effect of strong spin fluctuation, which might start to develop from well above the long-range ordering temperature in the present highly symmetric cubic crystal structure. On the other hand, the resistivity clearly changes at T_{N2} and T_{N1}, as shown in Fig. 7(b). Similar measurements were also carried out for other HM crystals. As presented in Fig. 7(c), the introduction of Co ions suppresses T_{N3} but enhances T_{N1}. T_{N2} is slightly enhanced for the 1% Co-substitution compound and then merges with T_{N3} at 2% Co content. T_{N1} also merges with T_{N2} at a Co concentration of $x = 0.05$.

As mentioned already, the HM ordering originates from the competing exchange interaction between the NN and the next-NN couplings,[10] or from the double-exchange interaction in these materials with negative charge transfer energy.[6] Application of uniform magnetic field may stabilize a state with FM moment and thereby change the spin configuration. The introduction of Co ions reinforces the FM interaction; therefore, the stability of the HM magnetic phases also depends on Co concentration sensitively. Figures 8(a) and 8(b) respectively show the temperature dependence of susceptibility and resistivity at different magnetic fields. With increasing the field, both T_{N3} and T_{N2} (indicated by downward arrows) clearly decrease, whereas T_{N1} (indicated by triangles) shifts toward higher temperature (Fig. 8(a)). Above 8 T, the magnetic anomaly at T_{N1} disappears or merges with T_{N2}. This observation is in agreement with the change found in the resistivity data in magnetic fields (Fig. 8(b)).

To further examine the field effect on the HM structures, magnetization and resistivity were measured at several fixed temperatures for a field range up to 14 T. Figure 9 shows some representative results at several temperatures. As shown in Fig. 9(a), with increasing field, anomalies (marked with arrows) are observed in magnetization curves. These critical field values are determined to be the points where the field derivative of magnetization shows a maximum. These transitions more evidently show up in the field dependence of resistivity.

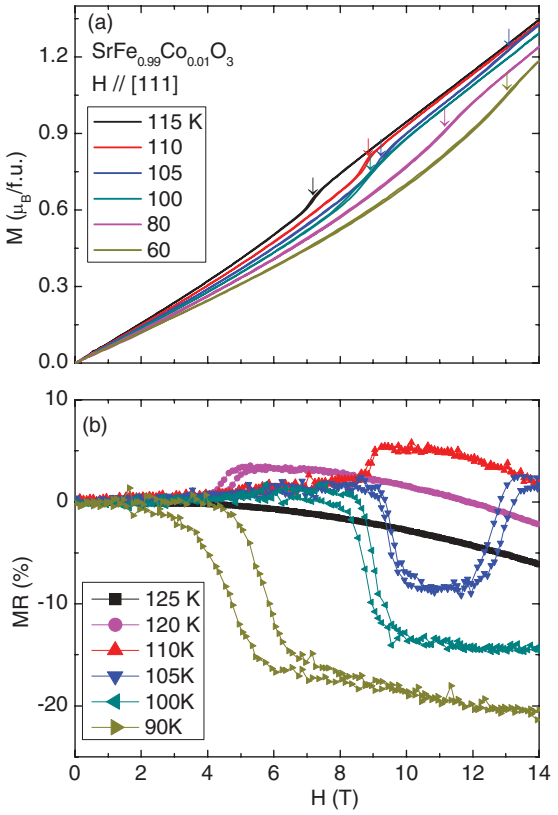

FIG. 9. (Color online) Field dependence of (a) magnetization and (b) magnetoresistance ratio $\{[\rho(H)-\rho(0)]/\rho(0)\}$ of $SrFe_{0.99}Co_{0.01}O_3$ at different temperatures. The transition fields as marked with arrows in (a) are determined as the point where the field derivative of magnetization shows a maximum.

Figure 9(b) presents the obtained magnetoresistance ratio as a function of field, and the corresponding transitions are clearly observed. For example, at 120 and 110 K, the MR sharply increases at about 4.5 and 8.8 T, respectively. As temperature decreases to 105 K, however, the MR firstly exhibits a large decrease around 9.5 T, and then abruptly increases near 12.5 T. Further lowering temperature to 100 or 90 K, only the transition at the lower field is observed in the field range we investigated. These field-induced transitions seem to accompany the field hysteresis and hence appear to be first order in nature.

All of these anomalies observed in magnetization and resistivity provide convincing evidences for field-induced spin structural transitions. On the basis of these detailed measurements, the phase diagram in the temperature vs field plane is obtained for $SrFe_{0.99}Co_{0.01}O_3$ as shown in Fig. 2(b). At low fields, three different HM phases (I, II, and III) are found. Accompanied by the phase transformations from I to II and from II to III, clear magnetic and resistive anomalies show up. At the transition from phase III to the PM phase, by contrast, only the magnetic anomaly is discerned. When the field is increased, two other magnetic phases (IV and V) emerge. These two phases are tentatively assumed to be conical-like spin states similar to B20-type compounds in magnetic fields.[1] Detailed spin structures for these phases remain to be solved in the future.

To systematically understand the evolution of helical spin states, we have also measured the field and temperature dependence of magnetization and resistivity for $SrFe_{0.98}Co_{0.02}O_3$ and $SrFe_{0.95}Co_{0.05}O_3$. Obtained phase diagrams are displayed in Fig. 2, together with the phase diagram of $SrFeO_3$, which is reproduced from Ref. 16 for comparison. Obviously, magnetic phases are largely affected by partial Co substitution. Only 1% Co content reduces the temperature windows of phases II and III by 20 K and 18 K at low fields, respectively. A similar suppression is also found for phase V. Moreover, the field value of the multicritical point among phases I, II, and IV decreases approximately from 14 to 9 T, and that of phases II, III, and V decreases from 12 to 6 T. When the Co content is increased to 2%, phases III and V disappear, and phase II is also suppressed significantly. The multicritical competition among phases I, II, and IV occurs at about 3 T. Furthermore, in the 5% Co-substituted crystal, phase II disappears, and only phases I and IV are present. In addition, the phase boundary between phases I and IV becomes rather low (<3 T), indicating that a conical state is easily stabilized in this compound. This phase diagram (Fig. 2 for $x = 0.05$) rather resembles those of conventional helimagnets. The observed variation in the phase diagrams together with the results of RSXD indicate that the HM phase I is more stabilized while periodicity of the helix gradually becomes longer as Co content is increased, and eventually the ground state is turned into the FM phase via the CG state.

As in the case of $SrFeO_3$, it is quite surprising and interesting that the HM structures in the simple cubic perovskite show up in such a large variety of magnetically distinct forms. A plausible origin might be sought in the multi-q states, e.g., the combination of the $\langle 111\rangle$-equivalent q-vectors, as in the case of the skyrmion lattice found in the MnSi and related helimagnets.[36–40] However, the rapid change in the phase diagram as a function of Co concentration contrasts with the case of MnSi-related materials,[40] where the phase diagram remains rather similar during the introduction of disorder. The difference may be ascribed to the difference in the relevant interaction (exchange interaction vs DM-interaction) and resultant length scale of the helix (several nm vs several tens of nm). The mystery of the versatile helimagnetic states in the simple cubic chemical lattice remains to be solved; nevertheless, the systematic behavior with Co concentration as demonstrated in this study will be of great use to future studies.

IV. CONCLUSION

High-quality single crystals of $SrFe_{1-x}Co_xO_3$ solid solution with simple cubic perovskite structure were prepared by a two-step method. With increasing Co concentration (x), the magnetism changes from a helimagnetic state with $0 \leqslant x \leqslant 0.05$ to a long-range ferromagnetic ordered state with $x \geqslant 0.2$ via an intermediate cluster glass state. While the system undergoes a series of magnetic transitions, all the compounds exhibit metallic behavior. What we found newly in this study are the following. Similar to $SrFeO_3$, three helimagnetic states (phases I, II, and III) are observed in zero magnetic field for the slightly Co-substituted sample $SrFe_{0.99}Co_{0.01}O_3$. With application of magnetic field, two phases, perhaps with conical spin structure (phases IV and V), are found. Only 1% Co substitution significantly reduces the temperature windows of

phases II, III, and V. In addition, the critical fields from helical-to-conical phase transitions are decreased considerably. When the Co content is increased to 2%, phases III and V disappear, and phase II is further suppressed. In the sample with 5% Co content, phase II also disappears, and only phases I and IV are left. Resonant soft x-ray diffraction measurement revealed that, in the course of this evolution of the magnetic phase diagram, the q-vector of the helix becomes gradually smaller. Thus, the transition to the ferromagnetic state is characterized by an increase in the periodicity of the helimagnetic structure. Detailed magnetic structures in the respective phases, possibly with some higher-order superstructures, should be explored in the future on the basis of the presently observed phase diagrams.

ACKNOWLEDGMENTS

We thank H. Sakai and T. Suzuki for help with magnetism and resistivity measurements. We also thank C. Q. Jin for useful discussions. This work was partly supported by the Funding Program for World-Leading Innovative R&D in Science and Technology (FIRST Program) on "Quantum Science on Strong Correlation" from the Japan Society for the Promotion of Science, and by Grants-in-Aid for Scientific Research (A) No. 21244049. The synchrotron radiation experiments were performed at the beamline 17SU in SPring-8 with the approval of RIKEN (Proposal No. 20100106, 20110016, and 20120018). Y.W.L. appreciates the support of the 100 Talents Project of the Chinese Academy of Sciences, China (Grant No. Y1k5019 × 51).

*Corresponding author: ywlong@iphy.ac.cn

[1] S. Mühlbauer, B. Binz, F. Jonietz, C. Pfleiderer, A. Rosch, A. Neubauer, R. Georgii, and P. Böni, Science **323**, 915 (2009).
[2] X. Z. Yu, Y. Onose, N. Kanazawa, J. H. Park, J. H. Han, Y. Matsui, N. Nagaosa, and Y. Tokura, Nature **465**, 901 (2010).
[3] T. Kimura, S. Ishihara, H. Shintani, T. Arima, K. T. Takahashi, K. Ishizaka, and Y. Tokura, Phys. Rev. B **68**, 060403(R) (2003).
[4] M. Mochizuki and N. Furukawa, Phys. Rev. B **80**, 134416 (2009).
[5] M. Takano, N. Nakanishi, Y. Takeda, S. Naka, and T. Takeda, Mater. Res. Bull. **12**, 923 (1977).
[6] M. Mostovoy, Phys. Rev. Lett. **94**, 137205 (2005).
[7] J. B. MacChesney and R. C. Sherwood, J. Chem. Phys. **43**, 1907 (1965).
[8] S. Kawasaki, M. Takano, and Y. Takeda, J. Solid State Chem. **121**, 174 (1996).
[9] T. Takeda, Y. Yamaguchi, and H. Watanabe, J. Phys. Soc. Jpn. **33**, 967 (1972).
[10] T. Takeda, S. Komura, and N. Watanabe, in *Ferrites*, edited by H. Watanabe, S. Iida, and M. Sugimoto (Center for Academic Publications, Tokyo, Japan, 1981), p. 385.
[11] T. Takeda, S. Komura, and H. Fujii, J. Mag. Mag. Mater. **31**, 797 (1983).
[12] Y. W. Long, Y. Kaneko, S. Ishiwata, Y. Taguchi, and Y. Tokura, J. Phys.: Condens. Matter **23**, 245601 (2011).
[13] Y. M. Zhao, R. Mahendiran, N. Nguyen, B. Raveau, and R. H. Yao, Phys. Rev. B **64**, 024414 (2001).
[14] A. Lebon, P. Adler, C. Bernhard, A. V. Boris, A. V. Pimenov, A. Maljuk, C. T. Lin, C. Ulrich, and B. Keimer, Phys. Rev. Lett. **92**, 037202 (2004).
[15] P. Adler, A. Lebon, V. Damljanovic, C. Ulrich, C. Bernhard, A. V. Boris, A. Maljuk, C. T. Lin, and B. Keimer, Phys. Rev. B **73**, 094451 (2006).
[16] S. Ishiwata, M. Tokunaga, Y. Kaneko, D. Okuyama, Y. Tokunaga, S. Wakimoto, K. Kakurai, T. Arima, Y. Taguchi, and Y. Tokura, Phys. Rev. B **84**, 054427 (2011).
[17] M. Reehuis, C. Ulrich, A. Maljuk, Ch. Niedermayer, B. Ouladdiaf, A. Hoser, T. Hofmann, and B. Keimer, Phys. Rev. B **85**, 184109 (2012).
[18] M. Abbate, G. Zampieri, J. Okamoto, A. Fujimori, S. Kawasaki, and M. Takano, Phys. Rev. B **65**, 165120 (2002).
[19] J. Okamoto, K. Mamiya, S.-I. Fujimori, T. Okane, Y. Saitoh, Y. Muramatsu, K. Yoshii, A. Fujimori, A. Tanaka, M. Abbate, T. Koide, S. Ishiwata, S. Kawasaki, and M. Takano, Phys. Rev. B **71**, 104401 (2005).
[20] A. Maignan, C. Martin, N. Nguyen, and B. Raveau, Solid State Sci. **3**, 57 (2001).
[21] S. Mathi Jaya, R. Jagadish, R. S. Rao, and R. Asokamani, Phys. Rev. B **43**, 13274 (1991).
[22] H. Sakai, J. Fujioka, T. Fukuda, D. Okuyama, D. Hashizume, F. Kagawa, H. Nakao, Y. Murakami, T. Arima, A. Q. R. Baron, Y. Taguchi, and Y. Tokura, Phys. Rev. Lett. **107**, 137601 (2011).
[23] H. Wadati, J. Okamoto, M. Garganourakis, V. Scagnoli, U. Staub, Y. Yamasaki, H. Nakao, Y. Murakami, M. Mochizuki, M. Nakamura, M. Kawasaki, and Y. Tokura, Phys. Rev. Lett. **108**, 047203 (2012).
[24] S. Partzsch, S. B. Wilkins, J. P. Hill, E. Schierle, E. Weschke, D. Souptel, B. Büchner, and J. Geck, Phys. Rev. Lett. **107**, 057201 (2011).
[25] S. Y. Zhou, Y. Zhu, M. C. Langner, Y.-D. Chuang, P. Yu, W. L. Yang, A. G. Cruz Gonzalez, N. Tahir, M. Rini, Y.-H. Chu, R. Ramesh, D.-H. Lee, Y. Tomioka, Y. Tokura, Z. Hussain, and R. W. Schoenlein, Phys. Rev. Lett. **106**, 186404 (2011).
[26] T. A. W. Beale, S. B. Wilkins, R. D. Johnson, S. R. Bland, Y. Joly, T. R. Forrest, D. F. McMorrow, F. Yakhou, D. Prabhakaran, A. T. Boothroyd, and P. D. Hatton, Phys. Rev. Lett. **105**, 087203 (2010).
[27] S. Smadici, J. C. T. Lee, S. Wang, P. Abbamonte, G. Logvenov, A. Gozar, C. Deville Cavellin, and I. Bozovic, Phys. Rev. Lett. **102**, 107004 (2009).
[28] S. Shin, M. Yonemura, and H. Ikawa, Mater. Res. Bull. **13**, 1017 (1978).
[29] A. Muñoz, C. de la Calle, J. A. Alonso, P. M. Botta, V. Pardo, D. Baldomir, and J. Rivas, Phys. Rev. B **78**, 054404 (2008).
[30] R. L. Toquin, W. Paulus, A. Cousson, C. Prestipino, and C. Lamberti, J. Am. Chem. Soc. **128**, 13161 (2006).
[31] T. Takeuchi, A. Chainani, Y. Takata, Y. Tanaka, M. Oura, M. Tsubota, Y. Senba, H. Ohashi, T. Mochiku, K. Hirata, and S. Shin, Rev. Sci. Instrum. **80**, 023905 (2009).
[32] R. D. Shannon, Acta Crystallogr. Sect. A **32**, 751 (1976).

[33] A. E. Bocquet, A. Fujimori, T. Mizokawa, T. Saitoh, H. Namatame, S. Suga, N. Kimizuka, Y. Takeda, and M. Takano, Phys. Rev. B **45**, 1561 (1992).

[34] R. H. Potze, G. A. Sawatzky, and M. Abbate, Phys. Rev. B **51**, 11501 (1995).

[35] M. Zhuang, W. Zhang, A. Hu, and N. Ming, Phys. Rev. B **57**, 13655 (1998).

[36] U. K. Rößler, A. N. Bogdanov, and C. Pfleiderer, Nature **442**, 797 (2006).

[37] A. Neubauer, C. Pfleiderer, B. Binz, A. Rosch, R. Ritz, P. G. Niklowitz, and P. Böni, Phys. Rev. Lett. **102**, 186602 (2009).

[38] C. Pappas, E. Lelièvre-Berna, P. Falus, P. M. Bentley, E. Moskvin, S. Grigoriev, P. Fouquet, and B. Farago, Phys. Rev. Lett. **102**, 197202 (2009).

[39] X. Z. Yu, Y. Onose, N. Kanazawa, J. H. Park, J. H. Han, Y. Matsui, N. Nagaosa, and Y. Tokura, Nature **465**, 901 (2010).

[40] C. Pfleiderer, T. Adams, A. Bauer, W. Biberacher, B. Binz, F. Birkelbach, P. Boni, C. Franz, R. Georgii, M. Janoschek, F. Jonietz, T. Keller, R. Ritz, S. Muhlbauer, W. Munzer, A. Neubauer, B. Pedersen, and A. Rosch, J. Phys.: Condens. Matter **22**, 164207 (2010).